# Computational Singular Perturbation Analysis of Two-Stage Ignition of Large Hydrocarbons†

**Andrei Kazakov, Marcos Chaos, Zhenwei Zhao, and Frederick L. Dryer***

*Department of Mechanical and Aerospace Engineering, Princeton University, Princeton, New Jersey 08544*

*Received: December 10, 2005; In Final Form: January 21, 2006*

Computational singular perturbation (CSP) analysis has been used to gain understanding of the complex kinetic behavior associated with two-stage ignition of large hydrocarbon molecules. To this end, available detailed and reduced chemical kinetics models commonly used in numerical simulations of *n*-heptane oxidation phenomena are directly analyzed to interpret the underlying fundamental steps leading to two-stage ignition. Unlike previous implementations of the CSP methodology, temperature is included as one of the state variables so that factors controlling ignition can be unambiguously determined. The analyzed models show differences in the factors contributing to the initial development and shutdown of the first ignition stage. However, during the second stage, both models show the importance of the degenerate branching decomposition of hydrogen peroxide, which contradicts some previous interpretations of this phenomenon.

## Introduction

Two-stage ignition (and related cool flame and negative temperature coefficient, NTC, phenomena) during low-temperature oxidation of large hydrocarbon molecules is a well-established process.[1−3] Emerging new combustion technologies (e.g., homogeneous charge compression ignition, HCCI, engines) as well as practical applications such as cool flame combustion in industrial fuel reforming processes[4] and associated safety hazards have strengthened the need to better understand the fundamental chemistry leading to two-stage ignition. Scientific interpretations of these phenomena date back several decades.[5−8] On the basis of the degenerate branching ideas introduced by Semenov,[5] initial isothermal kinetic models were developed[6] which failed to properly explain the observed two-stage behavior. The theory set forth by Sal'nikov[7] which introduced thermokinetic feedback (i.e., nonisothermal system) allowed Yang and Gray[8] to develop a chain-thermal model exhibiting negative temperature dependence. In their model,[8] the presence of an exothermic termination channel that dominates over branching as the system temperature increases is responsible for the NTC behavior.

The work of Benson[9] provided a basis for the current understanding of alkyl/alkylperoxy radical chemistry which drives the low-temperature oxidation of large hydrocarbon molecules. On the basis of his ideas, a comprehensive mechanistic analysis of two-stage ignition in terms of specific elementary processes was postulated. Among the major points of his analysis, Benson[9] suggested that (1) competition between the highly reversible oxygen addition reaction $R + O_2 \leftrightarrow RO_2$ and the reaction $R + O_2 \rightarrow$ olefin $+ HO_2$ (where R represents an alkyl radical) provides the switch from branching to nonbranching behavior as temperature increases and (2) for large hydrocarbon molecules, internal isomerization of alkylperoxy ($RO_2$) species leads to an intramolecular branching sequence at low temperatures.

Detailed as well as reduced reaction mechanisms of various levels of predictive ability describing low-temperature oxidation of large hydrocarbons (built around Benson's ideas[9]) started to appear in the late 1980s and are still under heavy development at present (see, for example, refs 10−16 for detailed[10−13] and reduced[14−16] models; it is noted, however, that many other mechanisms are currently available in the literature). Despite the availability of such reaction schemes capable of quantitative predictions of various experimental observations related to two-stage ignition phenomena, the detailed and unambiguous interpretation of these model predictions is still controversial.[17] This is primarily due to the complexity of the observed kinetic behavior as well as to the large size of the resulting detailed models which makes them difficult to interpret using conventional chemical kinetics tools (i.e., flux/sensitivity analysis).

The present study aims to develop a better interpretation of kinetic behavior related to two-stage ignition through the implementation of the computational singular perturbation method.[18] The kinetic models of Curran et al.[12] (detailed) and Peters et al.[15] (skeletal) for *n*-heptane oxidation are analyzed. *n*-Heptane was chosen since it is one of the most studied large hydrocarbon molecules due to its importance in practical combustion systems; it is a primary reference fuel for the octane rating of automotive gasolines as well as having a cetane number similar to that of conventional diesel fuels. Participating reactions driving both ignition stages are identified, and the fundamental differences between detailed and skeletal models are discussed.

## Methods

In this study, the computational singular perturbation (CSP) methodology[18] is used. While the most popular application of CSP is to generate reduced kinetic models,[19,20] this technique also provides the means to directly analyze complex kinetic systems and to identify specific processes/mechanisms responsible for observed macroscopic behavior.[18] The implementation of the CSP methodology used in the present study is briefly outlined below. The chemical kinetic reaction system may be represented by the following set of ordinary differential equations

$$\frac{d\mathbf{z}}{dt} = \mathbf{g}(\mathbf{z})$$

† Part of the special issue "David M. Golden Festschrift".

* To whom correspondence should be addressed. E-mail: fldryer@princeton.edu.

10.1021/jp057224u CCC: $33.50 
Published on Web 02/22/2006

where

$$\mathbf{z} = [\tilde{T}\ \ y_1\ \ y_2\ \ \ldots\ \ y_{n-1}\ \ y_n]^T$$

is the state variable vector, $\tilde{T}$ the normalized temperature, $y_i$ the species mass fractions ($n$ total), and $\mathbf{g}$ the overall reaction rate vector. The inclusion of temperature as one of the CSP state variables is essential for the direct analysis of thermokinetic feedback during autoignition; many previous CSP applications interested in mechanism reduction have not treated temperature as an independent variable. At any given time $t$, the rate vector can be differentiated (i.e., "perturbed") with respect to time, $d\mathbf{g}/dt = \mathbf{J}\cdot\mathbf{g}$, so that a local Jacobian matrix is defined, $\mathbf{J} = d\mathbf{g}/d\mathbf{z}$. One can, thus, perform the following decomposition on $\mathbf{J}$

$$\mathbf{J} = \mathbf{V}\Lambda\mathbf{V}^{-1}$$

where

$$\mathbf{V} = (\mathbf{v}_1\ \ \mathbf{v}_2\ \ \ldots\ \ \mathbf{v}_n\ \ \mathbf{v}_{n+1})$$

is the matrix of eigenvectors and $\Lambda$ the diagonal matrix containing eigenvalues. The differentiation essentially yields a system of linear, ordinary differential equations for $\mathbf{g}$. Through the use of the decomposition above, the rate vector can be represented as a sum of individual *modes*

$$\mathbf{g}(t + \Delta t) \approx \sum_{i=1}^{n+1} f_i \mathbf{v}_i \exp(\lambda_i \Delta t)$$

where $f_i$ is the mode amplitude (indicating the mode importance) and $\lambda_i$ the corresponding eigenvalue (indicating the mode time scale and physical behavior). It should be pointed out that because the Jacobian matrix is generally not symmetric, it may have complex eigenvalues and eigenvectors appearing as complex conjugate pairs. In the analysis, the complex conjugate pair of modes can be transformed into a pair of real modes in a manner similar to that described by Lu et al.[20]

The identified modes can be classified according to the sign of the real component of the system eigenvalues, $\mathrm{Re}(\lambda_i)$. The modes with negative $\mathrm{Re}(\lambda_i)$ are referred to as *stable* (decaying) modes, while the modes with positive $\mathrm{Re}(\lambda_i)$ are *unstable* (explosive) modes. *The explosive modes control the ignition behavior of the kinetic system.* In addition, the modes with nonzero $\mathrm{Im}(\lambda_i)$ represent *oscillatory* modes.

To identify contributions of individual reactions to a specific mode, the concept of *participation index* is introduced.[18] The rate vector $\mathbf{g}$ can be written as

$$\mathbf{g} = \sum_{j=1}^{R} r_j \mathbf{S}_j$$

where $r_j$ is the rate of the $j$th reaction ($R$ total) and $\mathbf{S}_j = \partial\mathbf{g}/\partial r_j$ the matrix of stoichiometric coefficients. Then, the participation index is defined as

$$\mathbf{P}_j = r_j \mathbf{V}^{-1}\cdot\mathbf{S}_j$$

where elements of vector $\mathbf{P}_j$ indicate the contributions of the $j$th reaction to the corresponding modes. For convenience, the participation indices for a given mode are usually normalized as described in ref 18.

CSP is a very versatile tool for studying ignition behavior. Identifying and following the explosive modes allows determination of the factors controlling ignition *directly* and *unambiguously* as compared with other approaches such as sensitivity analysis. Typical sensitivity analysis methods[22] can, indeed, compute time-dependent local sensitivity coefficients; however, this can only be done for either temperature or the mass fraction of a specific species (i.e., property dependent) and the analysis is indirect, that is, it is performed by perturbing a particular rate coefficient and monitoring the change in the observable of interest. The present CSP analysis has an advantage in comparison to such methods in that the entire thermokinetically coupled system is treated and perturbation is applied to the complete set of differential equations describing the kinetic system. This makes CSP ideal for the study of relevant stages during ignition processes.

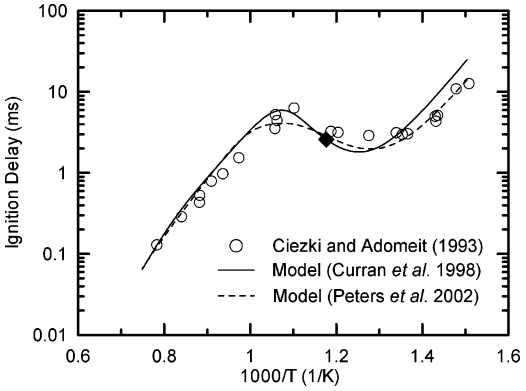


**Figure 1.** Ignition delay times as a function of temperature for a stoichiometric *n*-heptane/air mixture at 13.5 bar. The experiments of Ciezki and Adomeit[24] are compared against results obtained from detailed[12] and skeletal[15] models. The filled diamond shows the conditions chosen for this study (i.e., $T = 850$ K).

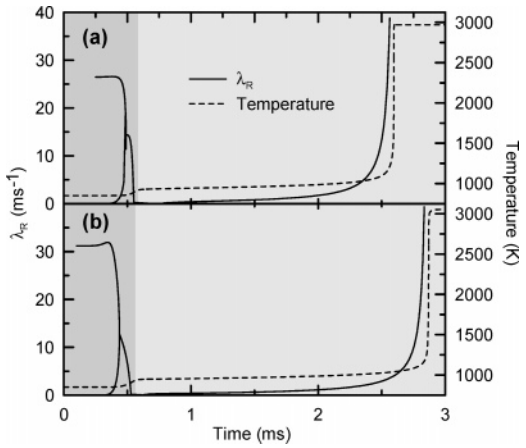


**Figure 2.** Temperature and eigenvalue spectrum time evolution for ignition simulations using the models of (a) Curran et al.[12] and (b) Peters et al.[15] Positive real eigenvalues are plotted corresponding to the leading modes (i.e., the modes with highest amplitudes) associated with ignition. The plots have been shaded to denote the presence of the two ignition stages.

In this work, an in-house CSP software package was developed and coupled with CHEMKIN[21] libraries to postprocess the results of kinetic simulations.[22] All eigenvalue analyses were performed using LAPACK library facilities.[23]

**Models and Case Study.** Two recent kinetic models of *n*-heptane oxidation were considered in this study. The first one was developed at Lawrence Livermore National Laboratory by Curran et al.[12] It consists of 561 species participating in 2539 elementary reactions and has been one of the most widely used both in kinetic modeling and as a reaction database. The other model considered was the skeletal mechanism of Peters et al.[15]

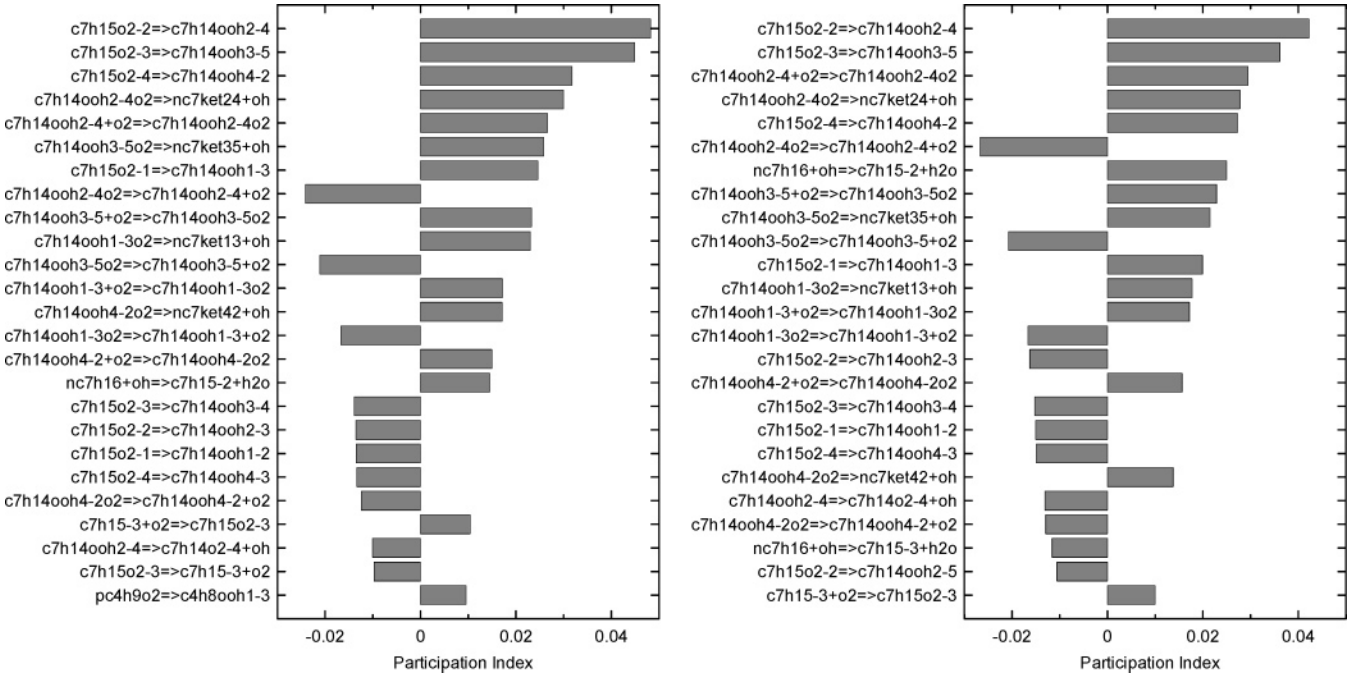


**Figure 3.** Makeup of explosive modes (fast mode, left; slow mode, right) at $t = 0.47$ ms (first stage) for the simulation shown in Figure 2a.

This model consists of only 35 species participating in 56 reactions. Its low-temperature ignition submechanism is heavily simplified, with only a few reactions describing the low-temperature branching sequence.

In the example presented in this study, the homogeneous adiabatic ignition of a stoichiometric *n*-heptane/air mixture at an initial pressure of 13.5 bar and temperature of 850 K was analyzed. As shown in Figure 1, these conditions correspond to the shock-tube ignition experiments of Ciezki and Adomeit[24] which are widely used for validation of low-temperature *n*-heptane mechanisms and the chosen initial temperature approximately corresponds to the middle of the NTC region.

## Results and Discussion

The temperature profiles for ignition of a stoichiometric *n*-heptane/air mixture at 13.5 bar and an initial temperature of 850 K computed using the mechanisms considered in this study[12,15] are presented in Figure 2. As expected, the two-stage ignition behavior is clearly observed. Also shown in Figure 2 are the real positive parts of the eigenvalues, $\lambda_R$, corresponding to the leading modes (i.e., the modes with the highest amplitudes) obtained from CSP analysis for the simulations. The presented results reveal an interesting pattern. In the beginning of the first stage, the ignition is characterized by a single explosive mode. As the system approaches the end of the first stage, in addition to the existing dominant explosive mode, another, slower, explosive mode with a lower amplitude appears. Immediately after its appearance, this new mode grows increasingly fast, while the original dominant mode becomes slower. This behavior continues until the two explosive modes collapse into a complex conjugate pair of explosive oscillatory modes. Then, the real part of this pair exhibits a rapid decrease passing through zero, so the modes lose their explosive nature, indicating the end of the first stage. After the end of the first stage, the system again develops a single dominant explosive mode that apparently controls the ignition runaway during the second stage. Below, this pattern is further analyzed by determining the contributing reactions to the relevant stages of ignition for the kinetic models considered in this study.

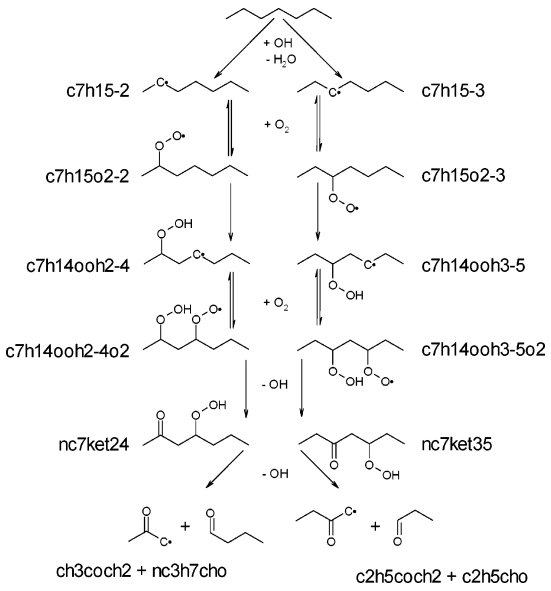


**Figure 4.** Main reaction pathways during low-temperature oxidation of *n*-heptane.

**Detailed Mechanism Analysis.** Figure 3 shows the participating reactions to the leading explosive modes during the developed first stage (see Figure 2a). In Figure 3 and other similar figures presented below, the participation index values are relative due to the normalization scheme[18] used in the analyses. These values present the importance of reactions promoting (positive) and inhibiting (negative) ignition. It can be seen that both modes share a similar reaction makeup indicating mode coupling. The first stage is governed by a low-temperature branching sequence (consistent with Benson[9]) with internal isomerization reactions of alkylperoxy radicals, such as c7h15o2-2 → c7h14ooh2-4 and c7h15o2-3 → c7h14ooh3-5, as the rate-controlling processes. Figure 4 shows the main reaction pathways during this low-temperature oxidation process. Due to bond strength and degeneracy, hydrogen abstractions from the second and third carbon atoms dominate. After molecular oxygen is added to these radicals, the alkylperoxy species

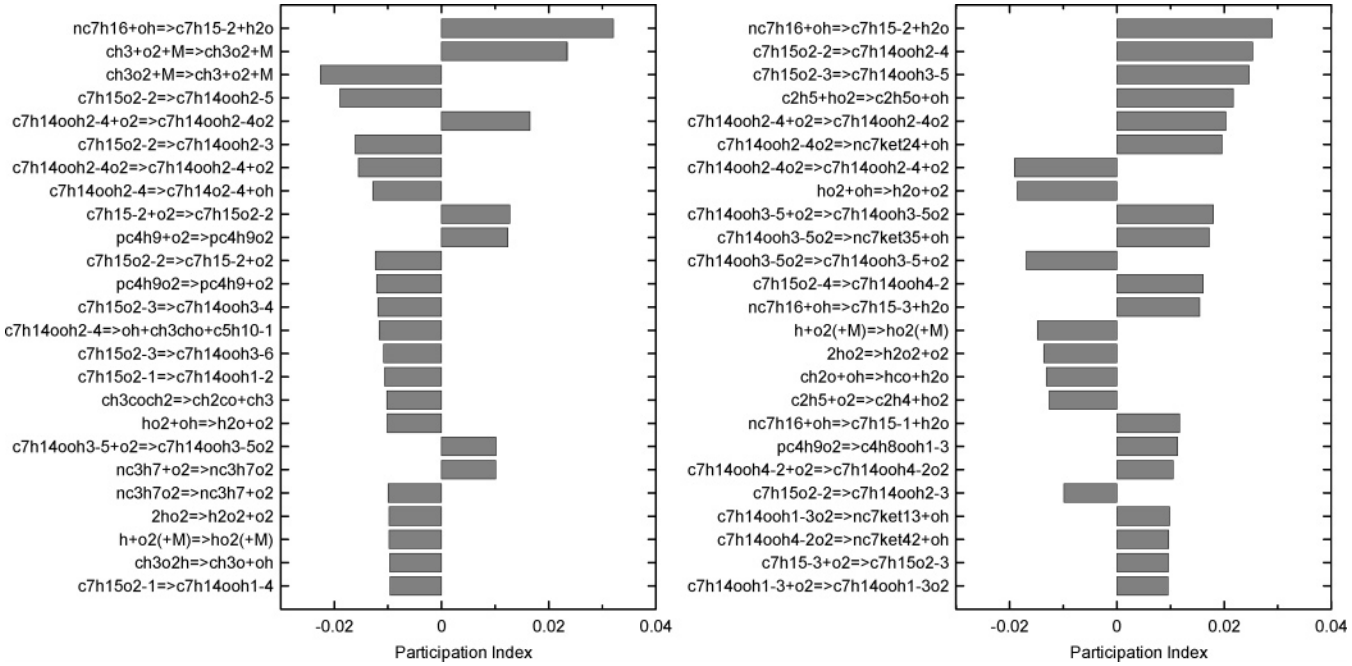


**Figure 5.** Makeup of oscillatory explosive modes (higher amplitude, left; lower amplitude, right) at $t = 0.55$ ms (end of first stage) for the simulation shown in Figure 2a.

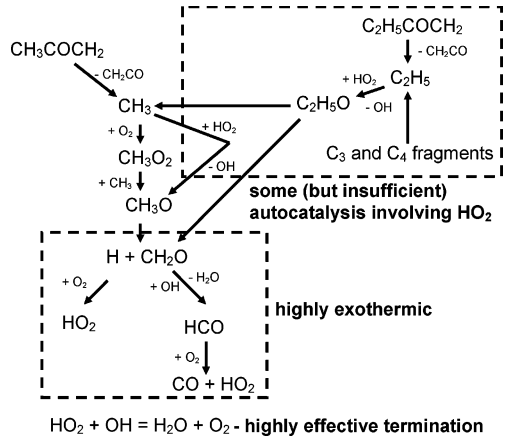


**Figure 6.** Heat flux analysis at the end of the first stage.

formed are mainly composed of c7h15o2-2 and c7h15o2-3. Isomerization then takes place with reactions including intermediate six-membered transition-state ring structures being the most important due to their low strain energy. Therefore, "2-4" and "3-5" isomerizations become the most significant steps, as shown in Figure 4. After isomerization, a second oxygen addition along with subsequent isomerization (forming keto-hydroperoxides) and decomposition occur releasing two hydroxyl radicals in the process, which provides chain branching.[3,9,12] The main products of this low-temperature branching sequence, as shown in Figure 4, are carbonyl and aldehyde species. The reactions that oppose the explosive behavior during the first stage (Figure 3) primarily include the decomposition of $O_2$QOOH adducts (i.e, products of the second oxygen addition, see Figure 4) back to QOOH and $O_2$ (for example, c7h14ooh2-4o2 → c7h14ooh2-4 + o2) and internal H-transfers forming QOOH species that have a radical site adjacent to the hydroperoxy group (such as c7h15o2-3 → c7h14ooh3-4). These latter species eventually lead to the formation of more stable conjugate olefins and $HO_2$.

Figure 5 shows the participating reactions at the end of the first stage. In addition to the above-mentioned pathways, it is

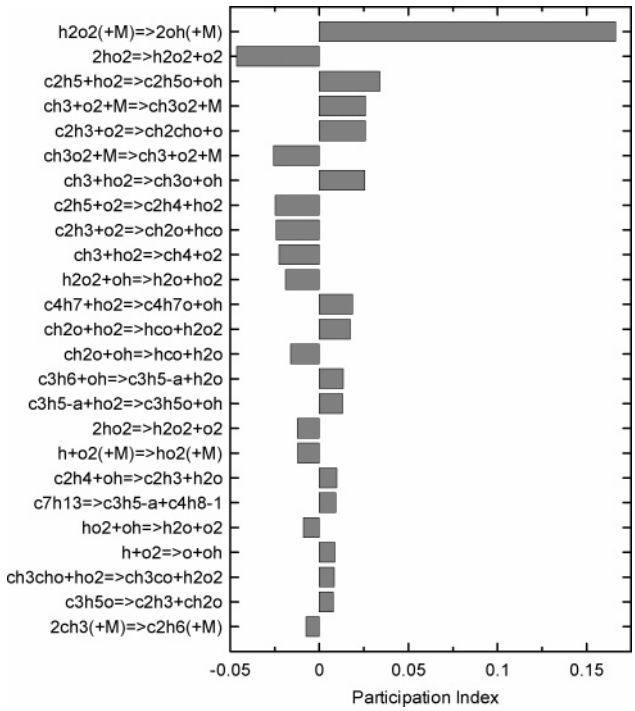


**Figure 7.** Makeup of the explosive mode at $t = 2.25$ ms (second stage) for the simulation shown in Figure 2a.

observed that competition for OH becomes more pronounced. Internal H-transfers that lead to formation of cyclic ethers (i.e., c7h15o2-2 → c7h15ooh2-5) and, especially, branching and termination reactions of small species related to concurrent formation and consumption of $HO_2$, such as $HO_2 + OH \rightarrow H_2O + O_2$, are the major contributors to the slowdown of the ignition process. In fact, the complementary reaction heat flux analysis shown in Figure 6 suggests that this process is associated with the emerging heat release coming from a sequence of exothermic steps involved in formation and oxidation of formaldehyde leading to the generation of $HO_2$. This sequence stems from the carbonyl species (i.e., ch3coch2 and c2h5coch2) formed

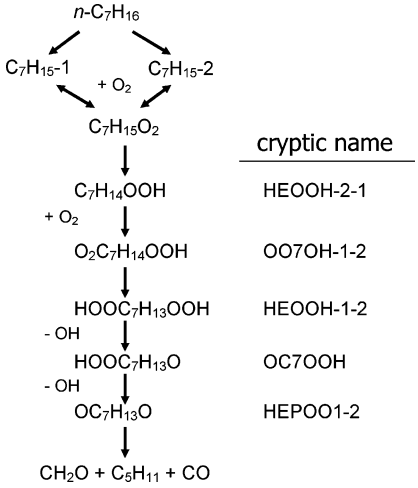


**Figure 8.** Low-temperature scheme of the skeletal mechanism of Peters et al.[15]

during low-temperature branching (see Figure 4). Although this process is extremely exothermic, it also produces large quantities of $HO_2$, which results in very effective chain termination via $HO_2 + OH \rightarrow H_2O + O_2$. This chain termination appears to be one of the major factors responsible for the process shutdown at the end of the first stage.

On the other hand, as can be seen from Figure 7, the single explosive mode responsible for the second stage of ignition is nearly exclusively driven by the degenerate branching reaction $H_2O_2 \rightarrow OH + OH$. This result is generally consistent with the conclusions of Westbrook[17] and Battin−Leclerc et al.[25] but contradicts the claim of Peters et al.[15] who interpreted the runaway at the second stage as a consequence of the sudden release of OH into the system once the fuel is fully depleted. As shown in Figure 7, no reactions of fuel and OH were found to have noticeable contributions to the explosive mode. Therefore, on the basis of the present CSP analysis, *the argument* of Peters et al.[15] can be conclusively *rejected* (as will be shown below, CSP analysis of the skeletal mechanism of Peters et al.[15] also identifies $H_2O_2$ decomposition as the key step driving the second ignition stage, in contradiction with their own interpretation). The other factors of importance during the second stage were found to be the termination reaction $HO_2 + HO_2 = H_2O_2 + O_2$ and a number of secondary branching and termination reactions involving $C_1$ and $C_2$ species.

**Skeletal Mechanism Analysis.** The low-temperature reaction scheme used in the reduced model of Peters et al.[15] is shown in Figure 8; only the eight steps shown in the figure describe the low-temperature oxidation process. Figure 9 shows contributing reactions during the developed first stage (see Figure 2b) obtained from CSP analysis. Similar to Figure 3, the leading modes show coupling (i.e., participating reactions are similar for both modes). Internal isomerization and ketohydroperoxide decomposition are the key rate-controlling reactions during the first stage. However, it is also seen that alkyl radical decomposition, which becomes important at high temperatures, strongly competes with $O_2$ addition at these intermediate temperatures. Furthermore, at the end of the first stage (Figure 10), ketohydroperoxide decomposition behaves drastically different between the two modes. These trends are essentially different from those observed when analyzing the detailed mechanism of Curran et al.[12] These differences can be attributed to the substantial variations in the rate coefficient/thermochemistry choices between the two models as well as to the simplifications made in generating the skeletal scheme;[15] for example, isomerizations leading to the formation of conjugate olefins and $HO_2$ or cyclic ethers were ignored, and all reactions after the first $O_2$ addition to the alkyl radicals were assumed irreversible (see Figure 8). However, Figure 10 shows the presence of small species reactions involving formaldehyde and $HO_2$ at the end of the first stage, similar to Figure 5.

On the basis of the results above, it is of interest to investigate the product yield at relevant stages during the ignition process. Figure 11 shows the species distribution obtained from the simulation using the skeletal mechanism.[15] As can be seen, the product makeup is comprised mainly by small molecules and strongly dominated by ethylene. The net heat release in the first stage is a result of the extensive reaction of the initial fuel to form water (highly exothermic), the oxidation of formaldehyde

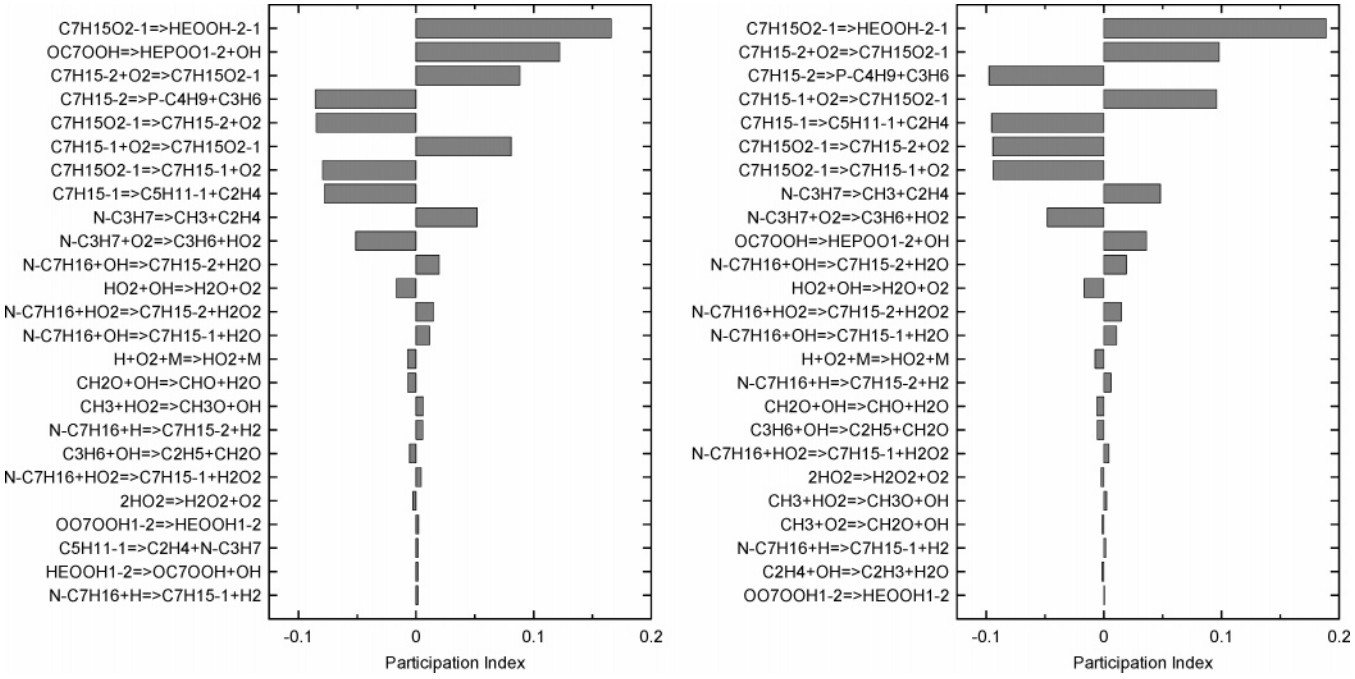


**Figure 9.** Makeup of explosive modes (fast mode, left; slow mode, right) at $t = 0.42$ ms (first stage) for the simulation shown in Figure 2b.

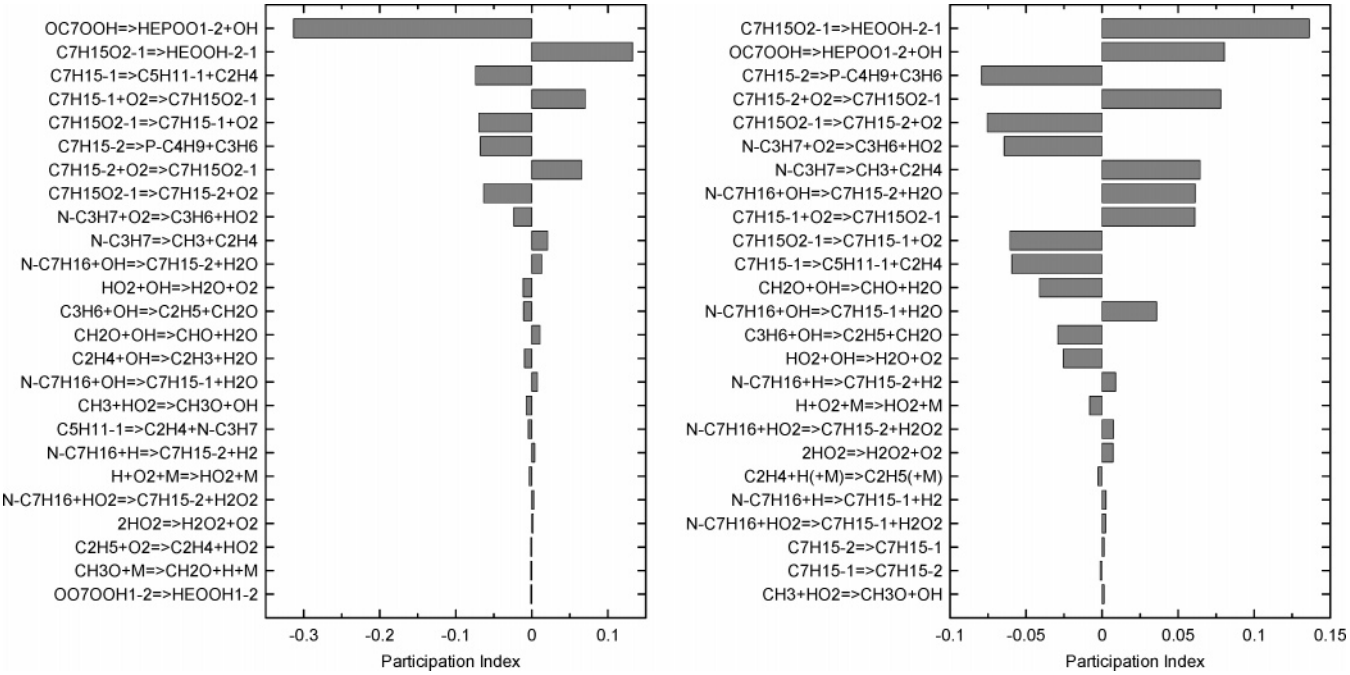


**Figure 10.** Makeup of explosive modes (higher amplitude, left; lower amplitude, right) at $t = 0.545$ ms (end of first stage) for the simulation shown in Figure 2b.

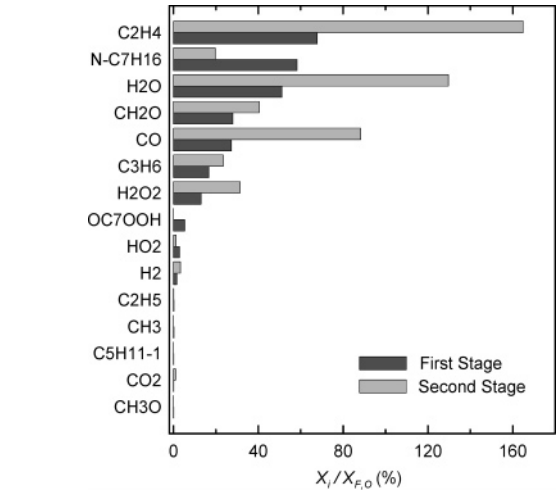


**Figure 11.** Species distribution at the end of the first stage ($t = 0.55$ ms) and during the onset of the second stage ($t = 2.60$ ms), using the reduced model.[15] Each species mole fraction ($X_i$) is given as a percentage of the initial fuel mole fraction ($X_{F,O}$).

to CO (exothermic), and the production of significant quantities of ethylene (endothermic) and formaldehyde formed from competing $\beta$-scission processes. In contrast, the species composition at the end of the first stage using the detailed model[12] shows considerable differences, as shown in Figure 12. The net heat release in this case essentially results from the limited oxidative conversion of the initial *n*-heptane. There is a considerably smaller amount of low carbon number products, particularly ethylene and formaldehyde formed, and consequently considerably less CO and water present. $\beta$-scission processes do not compete effectively with the oxygen addition channels. The amount of hydrogen peroxide produced is far smaller than that predicted using the skeletal mechanism. Instead, larger olefinic molecules along with cyclic ethers (QO), aldehydes, and carbonyl species are present. Thus, while both mechanisms yield similar characteristic ignition delay times and first stage heat release, Figure 12 shows that there is a substantial disparity in the product mixture present as the second stage of

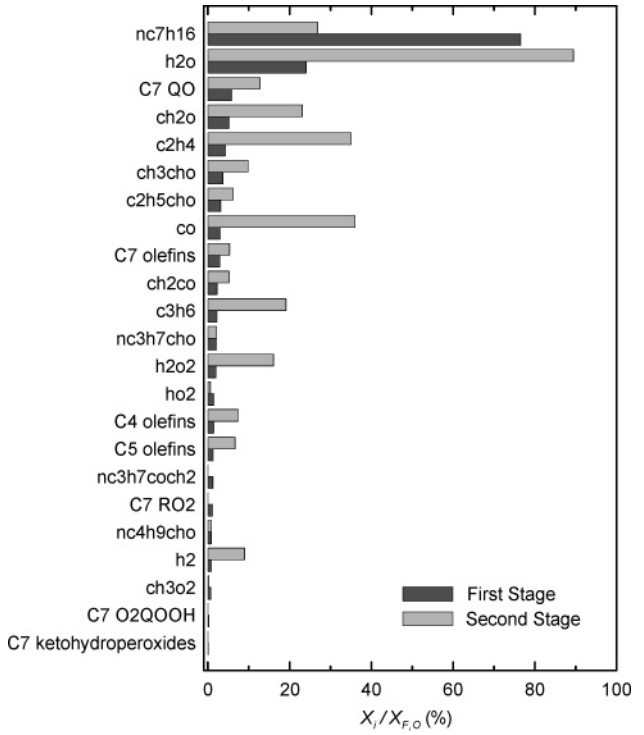


**Figure 12.** Species at the end of the first stage ($t = 0.55$ ms) and during the onset of the second stage ($t = 2.25$ ms) using the detailed model.[12] Each species mole fraction ($X_i$) is given as a percentage of the initial fuel mole fraction ($X_{F,O}$).

ignition begins. This disparity in product yields will likely result in very different modeling predictions of other phenomena important in engine combustion applications. For example, HCCI engine simulations where residual exhaust components and exhaust gas recirculation are likely to be present will show significantly different coupling in terms of perturbation of autoignition on the next power stroke. The presence of large amounts of ethylene obtained from the reduced model will also change flame speed properties in spark ignition engine simulations.

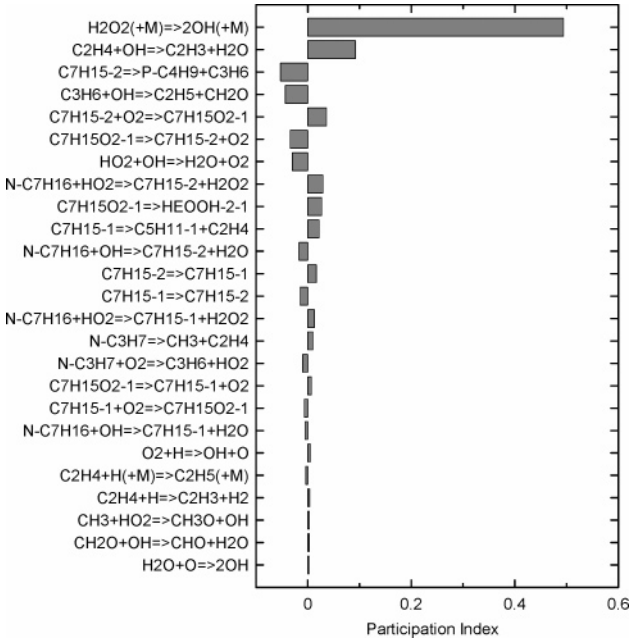


**Figure 13.** Makeup of the explosive mode at $t = 2.60$ ms (second stage) for the simulation shown in Figure 2b.

The second ignition stage, as shown in Figure 13, is, again (see Figure 7), driven by the decomposition of hydrogen peroxide. Reactions involving the parent fuel have no significant influence during the second stage. This result lends further support to the argument made above when analyzing the detailed mechanism. In fact, the reaction makeup of the explosive mode during the development of the second stage (i.e., from 0.55 to 3 ms, see Figure 2b) did not change from that shown in Figure 13. During this period, some fuel still remains in the system (Figure 11) and, yet, no fuel reactions with OH (as proposed by Peters et al.[15]) are important compared with the degenerate branching decomposition of $H_2O_2$, based on the CSP participation index data.

## Conclusions

Comprehensive analysis of a large-scale, detailed mechanism[12] and a skeletal, reduced mechanism[15] for low-temperature *n*-heptane oxidation has been performed. Conventional flux as well as computational singular perturbation (CSP) analyses have been used to interpret the causes of two-stage ignition behavior at high-pressure conditions. CSP has been demonstrated to have a strong potential for analyzing complex kinetic behavior associated with large kinetic systems as well as being an essential tool for conceptual mechanism cross-comparison. The analyses confirmed that the initial evolution toward ignition during the first stage is controlled by the accepted low-temperature branching sequence,[9] with internal isomerizations being the most prominent. CSP analysis shows the presence of a leading pair of explosive oscillatory modes during the first stage and a single explosive mode driving the second stage. The combined CSP/flux analysis suggests that one of the main factors causing the reaction slowdown at the end of the first stage is an exothermic but chain-terminating process involving the oxidation of formaldehyde, accompanied by the formation of $HO_2$.

It has been conclusively confirmed that chain-thermal runaway during the second stage of the ignition process is primarily governed by degenerate branching resulting from $H_2O_2$ decomposition. This result is consistent with recent analyses[17,25] but contradicts the interpretations offered by Peters et al.[15] The present CSP analyses of the Peters et al. model,[15] however, also identify hydrogen peroxide decomposition as the most significant reaction, negating their own proposal of an alternative cause. Moreover, the present results show that although the predicted overall heat release and ignition delay are similar for both detailed and reduced mechanisms, the product speciations are extremely different. The reduced mechanism produces a pool of small carbon number molecules dominated by ethylene and formaldehyde, whereas the detailed mechanism results in a significant fraction of initial fuel along with large olefins and partially oxygenated species. This illustrates the shortcomings in the generation of skeletal mechanisms based on limited validation targets.

**Acknowledgment.** This work has been supported by NASA Grant NCC3-375 and by the Chemical Sciences, Geosciences and Biosciences Division, Office of Basic Energy Sciences, Office of Science, U.S. Department of Energy under Grant No. DE-FG02-86ER13503.

## References and Notes

(1) Lewis, B.; von Elbe, G. *Combustion, Flames, and Explosions of Gases*, 3rd ed.; Academic Press: Orlando, FL, 1987.

(2) Glassman, I. *Combustion*, 3rd ed.; Academic Press: San Diego, CA, 1996.

(3) Griffiths, J. F. Presented at the European Combustion Meeting; Louvain-la-Neuve, Belgium, 2005; Plenary Lecture I.

(4) Hartmann, L.; Lucka, K.; Köhne, H. *J. Power Sources* **2003**, *118*, 286.

(5) Semenov, N. N. *Chemical Kinetics and Chain Reactions*; Oxford University Press: Oxford, U.K., 1935, and the original references therein.

(6) Frank-Kamenetskii, D. I. *Diffusion and Heat Transfer in Chemical Kinetics*; Plenum Press: New York, 1969, and the original references therein.

(7) Sal'nikov, I. E. *Zh. Fiz. Khim.* **1939**, *3*, 258.

(8) Yang, C. H.; Gray, B. F. *J. Phys. Chem.* **1969**, *73*, 3395.

(9) Benson, S. W. *Prog. Energy Combust. Sci.* **1981**, *7*, 125.

(10) Chevalier, C.; Warnatz, J.; Melenk, H. *Ber. Bunsen-Ges.* **1990**, *94*, 1362.

(11) Come, G. M.; Warth, V.; Glaude, P. A.; Fournet, R.; Battin-Leclerc, F.; Scacchi, G. *Proc. Combust. Inst.* **1996**, *26*, 755.

(12) Curran, H. J.; Gaffuri, P.; Pitz, W. J.; Westbrook, C. K. *Combust. Flame* **1998**, *114*, 1497 (also the 2004 version of the mechanism at http://www-cms.llnl.gov/combustion/combustion2.html).

(13) Ranzi, E.; Dente, M.; Goldaniga, A.; Bozzano, G.; Faravelli, T. *Prog. Energy Combust. Sci.* **2001**, *27*, 99.

(14) Bollig, M.; Pitsch, H.; Hewson, J. C.; Seshadri, K. *Proc. Combust. Inst.* **1996**, *26*, 729.

(15) Peters, N.; Paczko, G.; Seiser, R.; Seshadri, K. *Combust. Flame* **2002**, *128*, 38.

(16) Soyhan, H. S.; Mauss, F.; Sorusbay, C. *Combust. Sci. Technol.* **2002**, *174*, 73.

(17) Westbrook, C. K. *Proc. Combust. Inst.* **2000**, *28*, 1563, and the discussion section therein.

(18) Lam, S. H. *Combust. Sci. Technol*. **1993**, *89*, 375.

(19) Massias, A.; Diamante, D.; Mastorakos, E.; Goussis, D. A. *Combust. Flame* **1999**, *117*, 685.

(20) Lu, T.; Ju, Y.; Law, C. K. *Combust. Flame* **2001**, *126*, 1445.

(21) Kee, R. J.; Rupley, F. M.; Miller, J. A. *CHEMKIN II: A Fortran Chemical Kinetics Package for the Analysis of Gas-Phase Chemical Kinetics*; Sandia National Laboratories: Albuquerque, NM, 1989; SAND89-8009.

(22) Lutz, A. E.; Kee, R. J.; Miller, J. A. *SENKIN: A Fortran Program for Predicting Homogeneous Gas Phase Chemical Kinetics with Sensitivity Analysis*; Sandia National Laboratories: Albuquerque, NM, 1987; SAND87-8248.

(23) Anderson, E.; Bai, Z.; Bischof, C.; Blackford, S.; Demmel, J.; Dongarra, J.; Du Croz, J.; Greenbaum, A.; Hammarling, S.; McKenney, A.; Sorensen, D. *LAPACK Users' Guide*, 3rd ed.; SIAM: Philadelphia, PA, 1999.

(24) Ciezki, H.; Adomeit, G. *Combust. Flame* **1993**, *93*, 421.

(25) Battin-Leclerc, F.; Buda, F.; Fairweather, M.; Glaude, P. A.; Griffiths, J. F.; Hughes, K. J.; Porter, R.; Tomlim, A. S. Presented at the European Combustion Meeting; Louvain-la-Neuve, Belgium, 2005; Paper 16.